Generation of Localized Noninductive Current by Electron Cyclotron Waves on the DIII-D Tokamak

T. C. Luce,[1] Y. R. Lin-Liu,[1] R. W. Harvey,[2] G. Giruzzi,[3] P. A. Politzer,[1] B. W. Rice,[4] J. M. Lohr,[1]
C. C. Petty,[1] and R. Prater[1]

[1]*General Atomics, San Diego, California 92186-5608*
[2]*CompX, Del Mar, California 92014*
[3]*CEA-Centre d'Études de Cadarache, Saint Paul Lez Durance, France*
[4]*Lawrence Livermore National Laboratory, Livermore, California 94551-9900*
(Received 12 May 1999)

Localized currents due to electron cyclotron current drive have been measured for the first time in experiments on the DIII-D tokamak. The location of driven current in the plasma has been varied from near the center of the tokamak out to half of the minor radius. The measured current drive efficiency agrees with quasilinear Fokker-Planck calculations near the center and exceeds the predicted value with increasing minor radius. Reduction of the trapped electron fraction due to finite collisionality is a leading candidate to explain the discrepancy.

The experiments reported here represent the first direct measurements of localized, noninductive current generation by electron cyclotron waves in a high-temperature tokamak plasma. The motivations for this research are to supply the toroidal current necessary for plasma confinement in a tokamak by means other than the transformer action, and to allow feedback control of the current profile to extend the fusion performance beyond the stability limits found for inductively driven tokamaks [1]. These conditions can only be realized in steady state at high energy gain if the bulk of the current in the plasma is driven by self-generated currents [2] due to density and temperature gradients (bootstrap current), somewhat analogous to thermoelectric currents in metals. It is unlikely, however, that the bootstrap current will perfectly match the desired profile; therefore, a flexible, localized source of noninductive current will be needed for control. Current driven by absorption of electron cyclotron waves, as reported here, is a leading candidate to fulfill this role because the location of the driven current is easily controlled and these waves can be launched with high power density into the plasma with a remote launching structure. In addition to these practical considerations, these experiments provide a unique test of the electron dynamics where magnetic mirror trapping of electrons with low parallel velocity should be important. (Trapped electrons are those which are confined to the outward side of the tokamak due to conservation of energy and magnetic moment as they move in the spatially varying magnetic field.) The trapping effects have profound implications in many areas of magnetic confinement physics, and a clear local test of the theoretical treatment has not been carried out.

Two gyrotron oscillators at 110 GHz are the source of the electron cyclotron waves [3]. In the experiments reported here, approximately 1 MW of power is applied to the plasma for up to 1 s. The waves are launched at an angle with respect to the major radius to generate current parallel to the existing current [4]. Between discharges, the launched beam can be steered in the vertical direction and wave absorption takes place near the intersection of the ray trajectories and the second harmonic of the electron cyclotron frequency.

In previous experiments with off-axis electron cyclotron current drive (ECCD), the magnitude of the driven current was inferred from changes in the voltage at the plasma boundary required to maintain constant plasma current [5,6], providing no information about the location and magnitude of the driven current density. The advantage in the present experiments is that the internal magnetic fields are measured directly using motional Stark effect (MSE) spectroscopy [7] of the deuterium atoms injected by neutral beams. This allows detailed reconstructions of the magnetic configuration, specifically the poloidal flux function ψ, as a function of both space and time [8]. The current density along the magnetic field ($J_\parallel$) is determined from Ampère's law by spatial derivatives of ψ, while the time derivative of ψ on a surface of constant toroidal flux gives the parallel electric field ($E_\parallel$) from Faraday's law. The analysis is done in a Lagrangian system of equations to more easily account for voltages induced by plasma motion. Axisymmetry is assumed, and all of the kinetic quantities are assumed to be constant on a surface of given ψ due to the rapid parallel transport. The appropriate radial coordinate is ρ, which is the square root of the toroidal flux normalized to its edge value. The neoclassical Ohm's law is assumed to hold [9], which implies the noninductive current density J_{NI} is given by $J_\parallel - \sigma_{neo}E_\parallel$, where σ_{neo} is the conductivity given by neoclassical theory [10]. For this Ohm's law to hold, transport or transformation of magnetic flux due to magnetohydrodynamic instability cannot be present. Therefore, very quiescent discharges (no sawteeth or edge localized modes) which are slowly evolving

are required for these measurements. Low power neutral beam injection (NBI) is used to slow the resistive evolution and to acquire MSE data. The J_{NI} includes contributions from neutral beam current drive, the bootstrap current, and ECCD. To isolate the current density arising from ECCD (J_{EC}), the difference is made between the ECCD discharge and a fiducial discharge with NBI only. The inferred J_{NI} for the fiducial is corrected for changes in the bootstrap and neutral beam driven currents due to the differences in density (n), temperature (T), and Z_{eff} between the two discharges. This correction is small for the cases shown here.

Using this technique, clear examples of localized current generation are obtained near the magnetic axis and at the half radius, as shown in Fig. 1. Focusing first on the case with current driven near the magnetic axis, the $J_{\parallel}$ and loop voltage ($V_L \equiv 2\pi R_0 E_{\parallel}$, where R_0 is the geometric center for the flux surface) inferred from the magnetic reconstructions are shown in Figs. 1(a) and 1(b), respectively, for the ECCD case and the fiducial. A clear increase in $J_{\parallel}$ is observed in the ECCD case at $\rho = 0.15$, which is the expected resonance location. The loop voltage drops to 0 there, indicating the current is supplied

FIG. 1. The radial profiles of (a) $J_{\parallel}$, (b) V_L, (c) J_{NI}, and (d) J_{EC} for the case of near central ECCD (solid line) and NBI only (dashed line). The discharge parameters are $B = 1.76$ T, $I = 0.89$ MA. $\bar{n} = 1.7 \times 10^{13}$ cm^{-3}, $P_{NB} = 2.6$ MW, $P_{EC} = 1.1$ MW. Boxes (e)–(h) are the same profiles for the case of current drive near the half radius; the discharge parameters are $B = 1.86$ T, $I = 0.94$ MA. $\bar{n} = 1.8 \times 10^{13}$ cm^{-3}, $P_{NB} = 2.6$ MW, and $P_{EC} = 1.0$ MW. The curves without error bars in (d) and (h) are the Fokker-Planck calculations as explained in the text. For (d) this calculation is scaled by 0.25 to fit the experimental plot.

noninductively. The current density on axis drops as expected from flux diffusion acting to yield an equilibrium with constant V_L at all ρ. Note that in both cases V_L has not equilibrated, which prevents an accurate estimate of the change in the noninductive current from the change in V_L at the edge. The error bars shown are one standard deviation (1σ) random errors in the determination of $\partial\psi/\partial t$ which is the dominant source of random error. Error bars in the subsequent figures are these same errors propagated through the analysis. The profile of J_{NI} is shown for the ECCD discharge and its NBI fiducial in Fig. 1(c). The graphs are stopped at $\rho = 0.7$ because the carbon density measurements used to determine the effective ion charge (Z_{eff}) are not available outside of this radius. The peak J_{NI} occurs as expected near $\rho = 0.15$.

Finally, the radial profile of J_{EC} is clearly observed from the difference between the ECCD case and the fiducial, as shown in Fig. 1(d). The profile is well resolved in the sense that the peak is more than 3σ above zero and the value at half maximum is more than 2σ from the peak. The integrated current to $\rho = 0.3$ is 92 ± 29 kA. The uncertainty quoted is the integral of the uncertainty in J_{EC}, which is a conservative estimate. Also shown in Fig. 1(d) is the predicted J_{EC} from a quasilinear bounce-averaged Fokker-Planck calculation [11] using the measured n, T, Z_{eff}, and $E_{\parallel}$. The current in this profile is 97 kA, in good agreement with the experimental value. The theoretical prediction has a much narrower profile than the experimental profile. It is not possible at the present time to attribute this difference to either finite spatial resolution of the analysis technique or actual broadening of J_{NI} due to transport or other effects.

A clear demonstration of driven current at the half radius by the same technique is shown in Figs. 1(e)–1(h). The modification of $J_{\parallel}$ [Fig. 1(e)] is much less pronounced than in the previous case because J_{EC} is only about 20% of the total current density. The reduction in ECCD is expected due to lower temperature and increased trapped electron fraction. Still, it is possible to see a small increase in $J_{\parallel}$ near $\rho = 0.5$, and a corresponding decrease in $J_{\parallel}$ to the inside. Comparison of the V_L profiles [Fig. 1(f)] for the ECCD discharge and the fiducial clearly shows less inductive flux is required in the ECCD discharge. Using the same methodology described above, the inferred J_{NI} and J_{EC} are shown in Figs. 1(g) and 1(h). Note that the scale in Fig. 1(h) is an order of magnitude smaller than in Fig. 1(d). However, the peak is well resolved in the statistical sense, and the integrated current is 35 ± 13 kA.

The theoretical prediction from the Fokker-Planck calculations for this case falls well short of the measured value, as shown in Fig. 1(h). The difference in profile width is again apparent; however, there is also a significant discrepancy in the total driven current, which is predicted to be only 8 kA. A physical model which may explain this discrepancy will be introduced at the end of
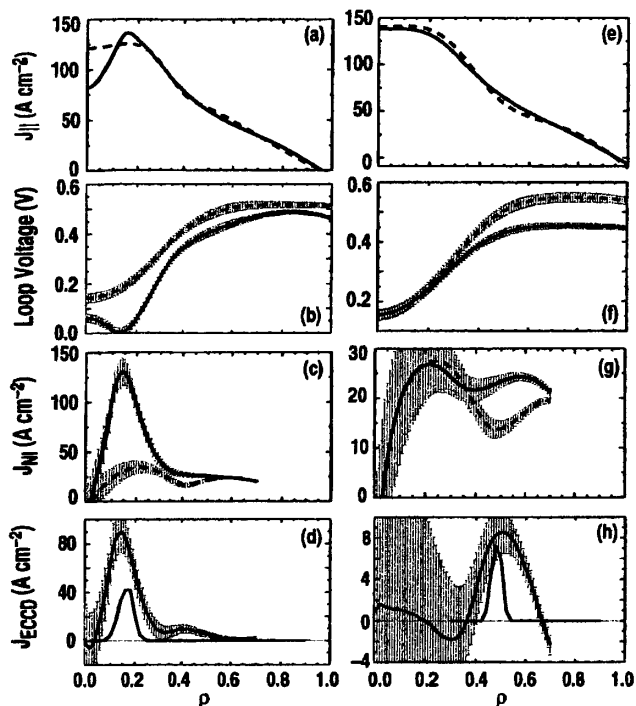
this Letter. It is felt that the difference between the theory and experiment does not arise from a systematic error due to finite spatial resolution of the analysis technique, since the analysis technique must account for the inductive flux balance in the discharge.

One of the goals of this series of experiments is to test the present predictive models of ECCD. To this end, two types of scans have been carried out—a scan of radial location of the driven current and a scan of the poloidal location of the driven current at fixed radius. The radial scan (fixed toroidal field and variable beam steering) tests the trapped electron and T dependence of the ECCD theory since T changes by a factor of 2 over the range $\rho = 0.1-0.5$. The poloidal scan (fixed beam steering and variable toroidal field) test the trapped electron dependence since the local trapped particle fraction varies from zero at the inboard midplane to maximum at the outboard midplane.

The radial scan shows no drop in measured efficiency with radius, in disagreement with theoretical predictions, as shown in Fig. 2. The comparison uses a dimensionless current drive efficiency

$$\zeta \equiv \frac{e^3}{\varepsilon_0^2} \frac{nIR}{PkT} \simeq 33 \frac{n_{20} I_A R_m}{P(\mathrm{W}) T(\mathrm{keV})},$$

where n_{20} is the local density in units of $10^{20} \ \mathrm{m}^{-3}$, I_A is the driven current in A, R_m is the major radius of the geometric center of the outermost flux surface in m, $P(\mathrm{W})$ is the absorbed power in W, and $T(\mathrm{keV})$ is the local electron temperature in keV. This efficiency is simply derived from normalizing the standard theoretical efficiency (J/p) to $nev_{\mathrm{th}}/nkT\nu_e$, where v_{th} and ν_e are the electron thermal velocity and collision frequency, respectively. This normalization should isolate the effects of the increasing trapped particle fraction in these scans. Three types of theoretical calculation are shown in Fig. 2—a linear

calculation [12], a quasilinear Fokker-Planck calculation [11], and the same Fokker-Planck calculation including the effects of a finite $E_\parallel$. The figure clearly shows that the predicted radial dependence in the normalized efficiency due to trapped electrons is strong, while the experimental data show essentially no variation. This trend in the theoretical predictions has been verified using an independent calculation [13]. In all but the centermost case where the power density is high, the quasilinear effects are expected to be small, and in all cases the measured $E_\parallel$ is predicted to have a minimal effect on the efficiency.

The two poloidal scans of the resonance location at $\rho \simeq 0.34$ and $\rho \simeq 0.47$ also show the measured efficiency exceeds the theoretical predictions. Figure 3 shows the measured ECCD efficiency along with the same theoretical models described above. The trend in the measured efficiency with poloidal angle is similar to that in the theoretical models, but with a substantial offset. The very large efficiency for the case with the largest poloidal angle prompted a modification of the Fokker-Planck code to allow an estimate of the current drive efficiency in the absence of trapped particles. This is shown by the open triangles in Fig. 3. This calculation sets a theoretical upper limit on the efficiency and provides a check that the measured efficiencies are physically reasonable.

The observation that the experimental ζ lies between the full calculation and the calculation with no trapping suggests that modification of the trapped particle boundary by finite collisionality may provide a physical explanation for the enhanced efficiency. [Collisionality (ν_*) is quantified as the ratio of the effective collision time to the bounce time of a particle with the thermal velocity.]
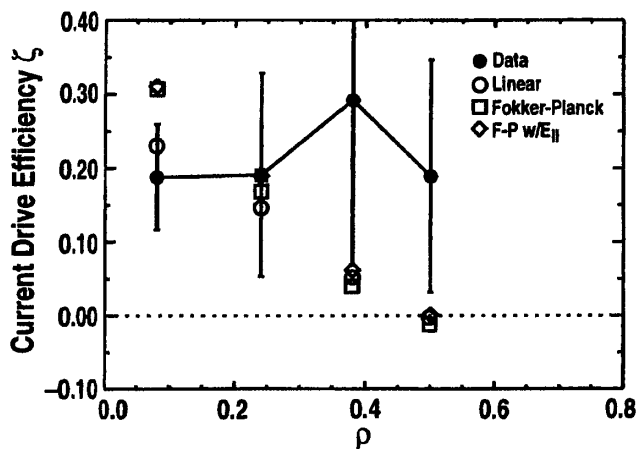
FIG. 2. Dimensionless current drive efficiency (defined in text) versus radius for fixed plasma parameters. The solid symbols are experimental measurements and open symbols are various theoretical model predictions.
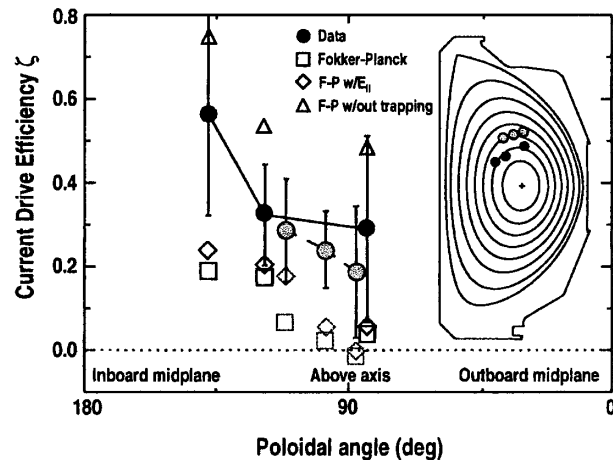
FIG. 3. Current drive efficiency versus poloidal angle (relative to the magnetic axis). The dark symbols joined by the solid line are for the scan at $\rho \simeq 0.30-0.37$ and the lighter symbols are for $\rho \simeq 0.44-0.50$. The inset shows the location of the current drive on a plot of contours of constant ψ. The vacuum vessel cross section is shown, and the center line is to the left.

The prediction of nearly zero current drive for $\rho = 0.5$ in Figs. 2 and 3 indicates that the "Ohkawa effect" [14] is the dominant velocity space effect. In the theoretical calculations, the velocity space is divided into two distinct regions—trapped and passing electrons. This boundary condition presumes zero collisionality, i.e., every electron, regardless of velocity, experiences the magnetic well. The Ohkawa effect is simply a realization that, in this ordering, the trapped particle region of velocity space acts as a short circuit from the cocurrent side of the distribution function to the countercurrent side, since the bouncing particles traverse this region in a fraction of a collision time. It is possible to get net negative current drive even when interacting with electrons initially carrying positive current.

Suppose now the effects of finite collisionality are introduced. The trapped particle region is effectively reduced by the probability that some particles will scatter into passing orbits before bouncing in the well. This reduction will occur preferentially at the lower velocities. From neoclassical theory [15], the first order correction for finite collisonality on quantities sensitive to trapped electrons is $\propto \sqrt{\nu_*}$, so even though $\nu_* \simeq 0.05$ in the cases shown in Fig. 3, the reduction in the effective trapped particle fraction is $\sim 20\%$ over all velocities and could be even higher in the region of velocity space where the ECCD is generated ($v \sim v_{\text{th}}$). The current is enhanced because the passing electrons carrying the current must now pitch-angle scatter through an additional region of velocity space in which they would have otherwise been trapped. This means that the electrons spend more time on the positive current side of the distribution and, hence, more current is obtained. Because the Ohkawa effect is subtractive, not multiplicative, this picture would explain the offset in the poloidal angle scans shown in Fig. 3. At present, this is simply a physical model, but work is in progress on theoretical calculations using a modified adjoint calculation without bounce averaging [16] and a Fokker-Planck calculation with full parallel dynamics [17].

In summary, clear evidence of localized current generation by EC waves has been demonstrated for the first time in experiments on the DIII-D tokamak. The measured current for cases with the current at $\rho \geq 0.3$ is significantly larger than the present state-of-the-art theoretical calculations predict. The leading candidate to explain this enhancement is finite collisionality which reduces the effects of the trapped electrons.

[1] A. D. Turnbull *et al.,* Phys. Rev. Lett. **74**, 718 (1995).
[2] R. J. Bickerton *et al.,* Nature (Phys. Sci.) **229**, 110 (1971).
[3] J. Lohr *et al.,* in Proceedings of the 23rd International Conference on Infrared and Millimeter Waves, Colchester, United Kingdom, 1998, edited by T. J. Parker and S. R. P. Smith, p. 269.
[4] N. Fisch, Rev. Mod. Phys. **59**, 175 (1987).
[5] A. Ando *et al.,* Phys. Rev. Lett. **56**, 2180 (1986).
[6] V. Erckmann and V. Gasparino, Plasma Phys. Controlled Fusion **36**, 1869 (1994).
[7] B. W. Rice *et al.,* Phys. Rev. Lett. **79**, 2694 (1997).
[8] L. L. Lao *et al.,* Nucl. Fusion **30**, 1035 (1990).
[9] C. B. Forest *et al.,* Phys. Rev. Lett. **73**, 2444 (1994).
[10] S. P. Hirshmann and D. J. Sigmar, Nucl. Fusion **21**, 1079 (1981).
[11] R. W. Harvey and M. C. McCoy, in *Proceedings of the IAEA Technical Committee Meeting, Montreal, 1992*, (IAEA, Vienna, 1993), p. 498.
[12] R. H. Cohen, Phys. Fluids **30**, 2442 (1987).
[13] G. Giruzzi, Phys. Fluids **31**, 3305 (1988).
[14] T. Ohkawa, General Atomics Report No. GA-A13847, 1976.
[15] F. L. Hinton and M. N. Rosenbluth, Phys. Fluids **16**, 836 (1973).
[16] O. Sauter, C. Angioni, and Y.-R. Lin-Liu, CRPP Report No. LRP 630/99, 1999 (to be published).
[17] O. Sauter, R. W. Harvey, and F. L. Hinton, Contrib. Plasma Phys. **34**, 169 (1994).